Spin Dynamics Investigation of Quasi-Frozen Spin Lattice for EDM Searches

E. Valetov[1,2], Yu. Senichev[2], and M. Berz[1]
On behalf of the JEDI Collaboration

[1]Michigan State University, East Lansing, MI 48824, USA
[2]Institute for Nuclear Physics (IKP), Forschungszentrum Jülich, Germany

September 27, 2016

2016 22nd International SPIN Symposium, Urbana-Champaign, Illinois

Outline

Frozen Spin (FS) Lattice

Particle spin alignment along momentum (frozen spin)

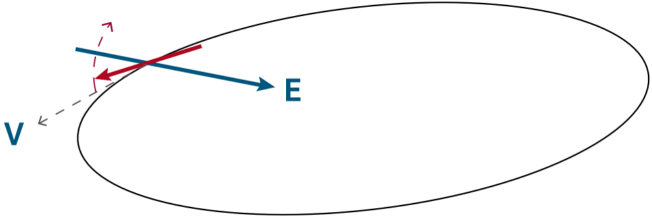

Radial E-field: torque on spin – rotation out of midplane

Quasi-Frozen Spin Technique

Thomas-BMT Equation

$$\frac{d\vec{S}}{dt} = \vec{S} \times \left(\vec{\Omega}_{MDM} + \vec{\Omega}_{EDM}\right)$$

where

$$\vec{\Omega}_{MDM} = \frac{e}{m}\left[G\vec{B} - \left(G - \frac{1}{\gamma^2 - 1}\right)\frac{\vec{E} \times \vec{\beta}}{c}\right]$$

and

$$\vec{\Omega}_{EDM} = \frac{e}{m}\frac{\eta}{2}\left[\frac{\vec{E}}{c} + \vec{\beta} \times \vec{B}\right]$$

Quasi-Frozen Spin (QFS) condition

$$\gamma G \Phi_B = \left[\frac{1}{\gamma}(1 - G) + \gamma G\right]\Phi_E$$

where Φ_B and Φ_E are the angles of momentum rotation due to magnetic and electric field respectively.

As a result, spin is *on average* aligned with momentum.

Quasi-Frozen Spin Technique

Illustration via analogy

© Horiabogdan | Dreamstime.com - Windy Road in the Forest photo.

Line of sight: the direction of momentum $\vec{p}$.

Momentary road direction: the direction of spin $\vec{s}$.

Quasi-Frozen Spin Lattices

Senichev 6.3 Lattice [SLL+15]

Lattice parameters

Length: 16,667 cm
Particles: deuterons
Kinetic energy: 270 MeV

System plot

Lattice structure

- 4 straight sections (light gray)
- 4 magnetic sections (light blue)
- 4 electrostatic sections (green)

Decoherence order suppression

- RF cavity: 1st and, partially, 2nd order (by mixing the particles relatively to the average field strength, averaging out $\triangle\gamma G$ for each particle).
- Sextupoles: remaining 2nd order component, (which is due to the average of $\triangle\gamma G$ being different for each particle).

Quasi-Frozen Spin Lattices

Senichev E+B Lattice [SBV+15]

Lattice parameters

Length: 14,921 cm
Particles: deuterons
Kinetic energy: 270 MeV

Lattice structure

- 2 straight sections (light gray)
- 4 magnetic sections (light blue)
- 2 E+B sections (orange)

System plot

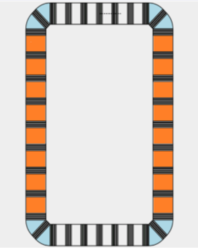

Decoherence order suppression

- RF cavity: 1st and, partially, 2nd order
- Sextupoles: remaining 2nd order component

The E+B static Wien Filter elements are used instead of the electrostatic deflector (1) to remove nonlinear components due to curved electrostatic element and (2) to simplify the system from the engineering perspective.

Quasi-Frozen Spin Lattices

Senichev BNL Lattice

Lattice parameters

Length: 14,585 cm
Particles: deuterons
Kinetic energy: 270 MeV

Lattice structure

- 2 straight sections (light gray)
- 2 curved E+B sections (light blue)

System plot

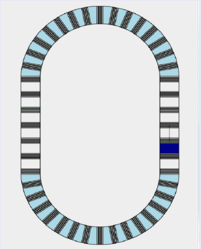

Decoherence order suppression

- RF cavity: 1st and partially 2nd order
- Sextupoles: remaining 2nd order component

The design of this lattice is based on the Frozen Spin method and uses a curved E+B element as proposed by the Storage Ring Electric Dipole Moment Collaboration [A+08].

Software

COSY INFINITY 9.2 [MB06]

We use COSY INFINITY for various spin tracking calculations, including

- the manual and automatic spin decoherence optimization by sextupole family strengths;
- the investigation of spin decoherence growth as a function of the number of turns; and
- the study of the effects of systematic errors on spin decoherence.

Wolfram Mathematica 10.4

We use Wolfram Mathematica notebooks for the following:

- the automated preparation of COSY INFINITY input files from templates using markers and regular expressions; and
- the storage, processing, quality assurance, and report generation using data from the COSY INFINITY output files.

Optimization of Sextupole Strengths

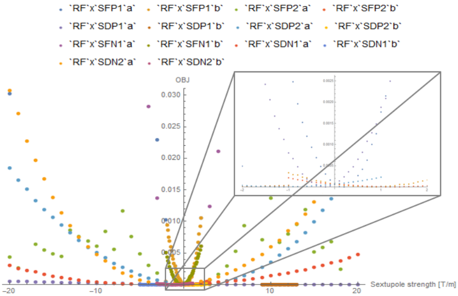

Optimization Context	Optimal Point	OBJ Value
\`RF\`x\`SFP1\`a\`	0.	0.0000662735
\`RF\`x\`SFP1\`b\`	0.2	3.01296×10^{-6}
\`RF\`x\`SFP2\`a\`	1.	9.43392×10^{-6}
\`RF\`x\`SFP2\`b\`	0.8	3.2609×10^{-7}
\`RF\`x\`SDP1\`a\`	11.	8.8197×10^{-7}
\`RF\`x\`SDP1\`b\`	10.6	5.23617×10^{-7}
\`RF\`x\`SDP2\`a\`	1.	4.79843×10^{-6}
\`RF\`x\`SDP2\`b\`	1.2	8.71622×10^{-7}
\`RF\`x\`SFN1\`a\`	0.	0.0000662735
\`RF\`x\`SFN1\`b\`	-0.2	1.5856×10^{-6}
\`RF\`x\`SDN1\`a\`	-3.	1.03277×10^{-6}
\`RF\`x\`SDN1\`b\`	-2.9	5.88324×10^{-7}
\`RF\`x\`SDN2\`a\`	-1.	2.22602×10^{-6}
\`RF\`x\`SDN2\`b\`	-1.2	3.48314×10^{-7}

The spin decoherence as a function of sextupole family strength.

1. We manually minimized spin decoherence up to ± 0.2 T/m by sextupole family strength in the $x-a$, $y-b$, and $l-\delta$ planes with a set of RF cavity frequencies and voltages.
2. We completed the optimization automatically using the LMDIF optimizer. At optimal values, the sextupole family strength typically has a 10^{-3} T/m error without a significant impact on the spin decoherence.

Reverse Spin Map

```
PROCEDURE SMR NAP LAP ; {REVERSES SPIN MAP NAP TO LAP}
   VARIABLE COD 1 NV ; VARIABLE NUM 1 ; VARIABLE I 1 ; VARIABLE J 1 ;
   VARIABLE MM NM1 3 3 ;
   VARIABLE T1 NM1 1 ; VARIABLE T2 NM1 1 ;
   VARIABLE FLG 1;
   NUM := MIN(TWOND,4) ;
   MATINV NAP MM;
   MM(1,3):=-MM(1,3); MM(2,3):=-MM(2,3);
   MM(3,1):=-MM(3,1); MM(3,2):=-MM(3,2);
   LOOP I 2 NUM 2 ; COD(I-1) := DD(I-1) ; COD(I) := -DD(I) ; ENDLOOP ;
   LOOP I NUM+1 NV ; COD(I) := DD(I) ; ENDLOOP ;
   IF ND>2 ; COD(5) := -DD(5) ; ENDIF ;
   LOOP I 1 3; LOOP J 1 3;
   T1(1):=MM(I,J);
   POLVAL 1 T1 1 COD NV T2 1 ;
   LAP(I,J):=T2(1);
   ENDLOOP; ENDLOOP;
ENDPROCEDURE ;
```

Screenshot of the procedure for reverse spin transfer map computation.

1. Consider a spin transfer map $M : X_i \rightarrow X_{i+1}$. Considering the nonlinear terms, M is a 3×3 matrix with differential algebra-valued elements. The inverse spin transfer map is $M^{-1} : X_{i+1} \rightarrow X_i$, where M^{-1} is the inverse matrix.
2. The time reversal results in the sign change of momentum (coordinates a and b) and the longitudinal offset (coordinate l) [Ber99, p.147].

Error Field Implementation

```
PROCEDURE RSY ANG; {SPIN KICK IN X-Z PLANE}
VARIABLE I 1; VARIABLE J 1;
{Set rotation matrix}
    UMS;
    LOOP I 1 3; LOOP J 1 3; SSCR(I,J):=0*DD(1);
    ENDLOOP; ENDLOOP;
    SSCR(2,2):=1+0*DD(1);
    SSCR(1,1):=COS(ANG)+0*DD(1);
    SSCR(1,3):=-SIN(ANG)+0*DD(1);
    SSCR(3,1):=SIN(ANG)+0*DD(1);
    SSCR(3,3):=COS(ANG)+0*DD(1);
{Update}
LOCSET 0 0 0 0 0 0; CE:='RSY'; DR:=0; UPDATE 1 1 1;
ENDPROCEDURE;
```

Screenshot of the procedure for a spin kick element.

According to the Thomas-BMT equation, a small perturbation of the magnetic field acts, to the first order, as a small rotation on the spin vector.

We implemented field errors as small, normally distributed spin kicks applied to the magnetic dipoles or combined E+B elements. The spin elements are interposed automatically into the COSY INFINITY code using one of the Mathematica notebooks.

Spin Decoherence with Optimized Sextupole Strengths

Spin decoherence versus the number of turns

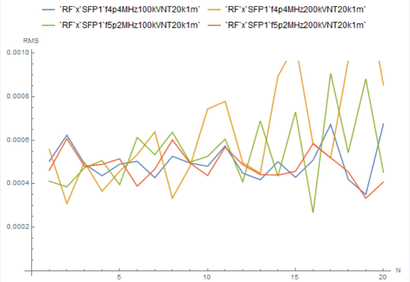

The spin decoherence versus the number of turns, Senichev 6.2 lattice, in plane, fringe field mode on (FR3), optimized by SFP1 sextupoles, up to 420 thousand turns.

Primary findings of the spin decoherence study

1. With an optimized sextupole family strength, the spin decoherence often remains in the same range for at least 5×10^5 turns.
2. The QFS structure decoherence is at least as good as, or better than, that of a FS structure decoherence.

Spin Decoherence Dynamics with Sextupole Optimization

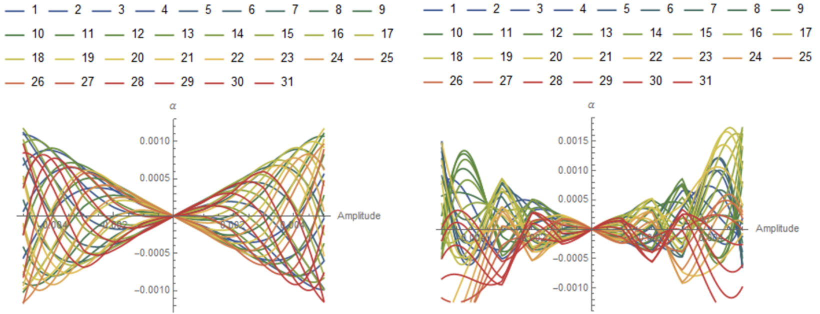

Examples of the time evolution of spin angle α (in $x - z$ plane, relative to reference particle) versus spacial amplitude.

- Both plots show conically bounded oscillations that are due to the energy averaging by the RF cavity.
- The plot on the left shows regular motion after the effective spin decoherence optimization by sextupole family strength. On the right, the optimization was not as effective.

Systematic Errors due to Magnet Rotational Misalignments

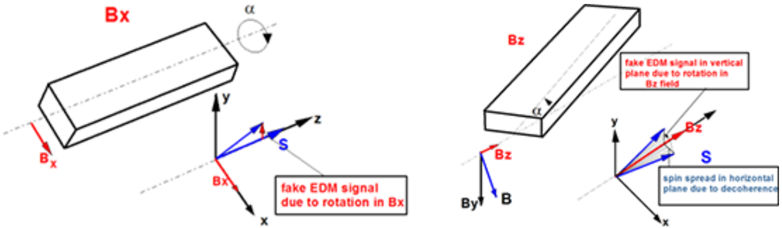

The rotational magnet misalignments, B_x and B_z error field components.

We studied the effect of rotational magnet misalignments on spin dynamics, namely spin decoherence and frequencies of rotation in a vertical plane, in QFS and FS structures. The error field components B_x and B_z are the most relevant to the detection of an EDM signal.

Mitigation of B_x and B_z Error Components

Clockwise (CW) and counterclockwise (CCW) lattice traversal

- We propose to track polarized particle bunches in the QFS/FS lattices in both CW and CCW directions.
- We consider the CW direction to be forward and the CCW direction to be reverse.
- We use the fact that in the linear approximation the reverse spin transfer map coincides with the inverse spin transfer map.

B_x error field component

- Rotation frequencies are $\Omega_x^{CW} = \Omega_{Bx}^{CW} + \Omega_{EDM}$ and $\Omega_x^{CCW} = -\Omega_{Bx}^{CCW} + \Omega_{EDM}$ in the vertical plane and $\Omega_y = 0 + \langle \delta\Omega_{decoh} \rangle$ in the horizontal plane.
- It is necessary to (1) minimize the decoherence in the vertical plane $\sigma_{\Omega_{Bx}}$ the same way as in the horizontal plane using the RF cavity and sextupole families and (2) minimize $\left|\Omega_{Bx}^{CW} - \Omega_{Bx}^{CCW}\right|$ by calibrating B^{CCW} to B^{CW} in the horizontal plane, where there is no EDM signal, using spin precession.
- Rotation frequency due to EDM is obtained by $\Omega_{EDM} = \left(\Omega_x^{CW} + \Omega_x^{CCW}\right)/2$.

Mitigation of B_x and B_z Error Components

B_z error field component

- The method of error field component mitigation for B_z is not applicable to B_x.
- We have to minimize Ω_{B_z} to $\sim 10^{-9} \frac{rad}{sec}$ using additional trim coils.

Outcome of the B_x and B_z error component mitigation method

- Using the error component mitigation method outlined here, a realistic Fermi estimate of measurement accuracy for Ω_{EDM} is 10^{-4} to 10^{-5} rad/sec.
- As a result, the accuracy of EDM signal measurement in one run is 10^{-24} to 10^{-25} $e \cdot cm$.
- The accuracy of the EDM signal measurement after one year of measurement may be 10^{-29} to 10^{-30} $e \cdot cm$.

Vertical Spin Decoherence, Approximate QFS/FS

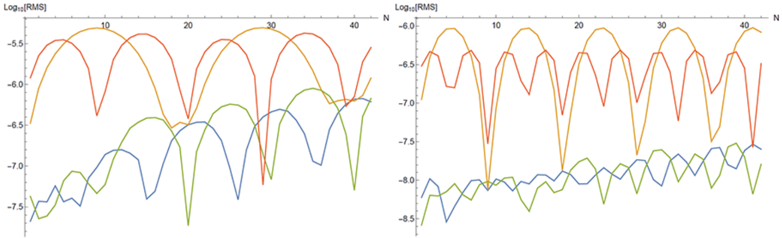

The vertical spin decoherence versus the number of turns, E+B lattice (left plot) and BNL lattice (right plot), optimization by the SDP sextupole family, and approximate QFS/FS (no corrective spin kick).

- With optimization by the SDP sextupoles, for the CW direction with error field components B_x (blue) and B_z (green), the vertical spin decoherence grows to $\sim 10^{-6}$ *rad* for the E+B lattice and $\sim 10^{-7.5}$ *rad* for the BNL lattice in 420 thousand turns.
- With optimization by the SDP sextupoles, for the CCW direction with error field components B_x (orange) and B_z (red), the vertical spin decoherence has the upper bound of $\sim 10^{-5}$ *rad* for the E+B lattice and $\sim 10^{-6}$ *rad* for the BNL lattice in 420 thousand turns.

Vertical Spin Decoherence, Exact QFS/FS

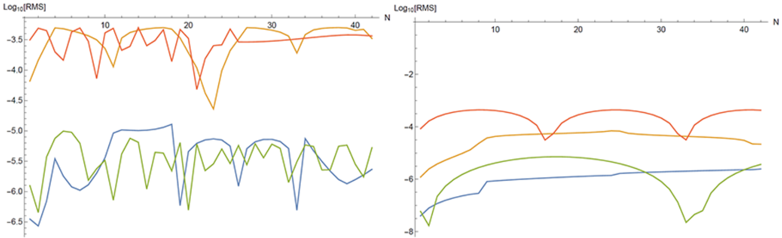

The vertical spin decoherence versus the number of turns, E+B lattice (left plot) and BNL lattice (right plot), optimization by the SDP sextupole family, exact QFS/FS (1x corrective spin kick).

- With optimization by the SDP sextupoles, for the CW direction with error field components B_x (blue) and B_z (green), the vertical spin decoherence has the upper bound of $\sim 10^{-5}$ *rad* for the E+B lattice and $10^{-6.5}$ to 10^{-5} *rad* for the BNL lattice in 420 thousand turns.
- With optimization by the SDP sextupoles, for the CCW direction with error field components B_x (orange) and B_z (red), the vertical spin decoherence has the upper bound of $\sim 10^{-3}$ *rad* for the E+B lattice and 10^{-4} to 10^{-3} *rad* for the BNL lattice in 420 thousand turns.

Summary of Calculation Results and Conclusion I

1. When a spin kick is used for the exact QFS/FS, the vertical spin decoherence in both lattices is about 10 to 10^2 higher, partly due to the spin rotation in the horizontal plane that effectively acts as an oscillation factor in the vertical spin motive force component in case of inexact QFS/FS.
2. Because the sextupoles were optimized for the CW lattices, the vertical spin decoherence is somewhat higher for the CCW direction.
3. Some of the apparent periodic spikes in spin decoherence are due to the use of the spherical coordinate system for the spin decoherence measure.
4. With an optimized sextupole family strength and with exact QFS/FS (via corrective spin kick), the vertical spin decoherence due to systematic errors often remains in the same range for at least 5×10^5 turns in both E+B (QFS) and BNL (FS) lattices.

Summary of Calculation Results and Conclusion II

5. Based on the systematic errors study data, the difference between the E+B (QFS) and BNL (FS) lattices is:
   1. quantitatively within about an order or two; and
   2. qualitatively appears to be insignificant.
6. The systematic errors study is ongoing and will yield additional results.
7. In the context of the systematic errors study, we will study the vertical spin motion and spin decoherence with B_x and B_z error field components while:
   1. slightly varying and optimizing the QFS/FS condition measure through the electrostatic and magnetic field strengths; and
   2. tracking the particle bunches for a larger number of turns.
8. We will (a) optimize the FS and QFS lattices by all sextupole families simultaneously using DA normal form methods and (b) use particle bunches with 6d distribution in phase space.

Endnotes I

D. Anastassopoulos et al., *AGS proposal: Search for a permanent electric dipole moment of the deuteron nucleus at the 10-29 e · cm level*, BNL Report, Brookhaven National Laboratory, U.S.A., April 2008, goo.gl/1K1TNq.

Martin Berz, *Modern map methods in particle beam physics*, Advances in Imaging and Electron Physics, Academic Press, San Diego, CA, 1999.

Kyoko Makino and Martin Berz, *COSY INFINITY version 9*, Nuclear Instruments and Methods in Physics Research, Section A: Accelerators, Spectrometers, Detectors and Associated Equipment **558** (2006), no. 1, 346–350.

Endnotes II

- Yurij Senichev, Serge Andrianov, Martin Berz, Stanislav Chekmenev, Andrei Ivanov, Bernd Lorentz, Jörg Pretz, and Eremey Valetov, *Systematic errors investigation in frozen and quasi-frozen spin lattices of deuteron EDM ring*, Proceedings of IPAC 2016, Busan, Korea, 2016, THPMR005.

- Yurij Senichev, Martin Berz, Eremey Valetov, Stanislav Chekmenev, Serge Andrianov, and Andrei Ivanov, *Investigation of lattice for deuteron EDM ring*, Proceedings of ICAP 2015, Shanghai, China, 2015, MODBC4.

- Yurij Senichev, Andreas Lehrach, Bernd Lorentz, Rudolf Maier, Serge Andrianov, Andrei Ivanov, Stanislav Chekmenev, Martin Berz, and Eremey Valetov, *Quasi-frozen spin method for EDM deuteron search*, Proceedings of IPAC 2015, Richmond, VA, 2015, MOPWA044.

Endnotes III

Eremey Valetov, Martin Berz, and Yurij Senichev, *Search for the optimal spin decoherence effect in a QFS lattice*, Proceedings of ICAP 2015, Shanghai, China, 2015, THDBC2.

Acknowledgments

- This material is based upon work supported by the U.S. Department of Energy, Office of Science, Office of High Energy Physics under Award Number DE-FG02-08ER41546.
- This research used resources of the National Energy Research Scientific Computing Center, a DOE Office of Science User Facility supported by the Office of Science of the U.S. Department of Energy under Contract No. DE-AC02-05CH11231.
- The authors would like to thank the computing support staff at the Department of Physics and Astronomy of Michigan State University for their assistance.


Thank you!